Journal of Computational Physics 229 (2010) 5564–5572

Contents lists available at ScienceDirect

Journal of Computational Physics

journal homepage: www.elsevier.com/locate/jcp

Unlike-particle collision operator for gyrokinetic particle simulations

R.A. Kolesnikov [a,*], W.X. Wang [b], F.L. Hinton [c]

[a] Los Alamos National Laboratory, Los Alamos, NM, USA
[b] Plasma Physics Laboratory, Princeton University, NJ, USA
[c] University of California, San Diego, CA, USA

ARTICLE INFO

Article history:
Received 18 October 2009
Received in revised form 17 March 2010
Accepted 12 April 2010
Available online 18 April 2010

Keywords:
Gyrokinetics
Magnetized plasmas
Plasma kinetic equations

ABSTRACT

Plasmas in modern tokamak experiments contain a significant fraction of impurity ion species in addition to main deuterium background. A new unlike-particle collision operator for δf particle simulation has been developed to self-consistently study the non-local effects of impurities on neoclassical transport in toroidal plasmas. A new algorithm for simulation of cross-collisions between different ion species includes test-particle and conserving field-particle operators. The field-particle operator is designed to enforce conservation of number, momentum and energy. It was shown that the new operator correctly simulates the thermal equilibration of different plasma components. It was verified that the ambipolar radial electric field reaches steady state when the total radial guiding center particle current vanishes.

1. Introduction

In present advanced tokamak experiments the improved confinement regime is achieved by reducing the turbulent transport in the ion channel. To understand the performance of such toroidal devices, the experimental data is normally compared with irreducible neoclassical transport level. While neoclassical theory has been well developed [1–3], there is need for direct numerical solution of the drift-kinetic equations globally, from the magnetic axis to the plasma boundary, with appropriate boundary conditions. This is necessary if one needs to capture non-local physics near magnetic axis or sharp profile gradients where basic assumptions of most local theories are violated. Also, the large scale ambipolar electric field must be self-consistently calculated by solving the Poisson equation. Self-consistency of the electric field, a feature absent from neoclassical theories, is important to maintain transport ambipolarity. While local neoclassical transport in axisymmetric systems, like tokamaks, is intrinsically ambipolar, non-local effects require constraint on the electric field to maintain ambipolarity [4]. In addition to main ion species, which is normally deuterium, most of experimentally relevant plasmas contain one or more ion species. Consequently, impurity particles can make a significant contribution to main deuterium heat flux indirectly by producing additional cross-species collisions.

In this paper we address the development of an unlike-particle collision operator for δf particle simulation technique. In addition to a test-particle operator, we describe a new field-particle operator which conserves particle number, energy and momentum. This work generalizes the like-particle collision operator developed in Ref. [5] to a system which involves particles with different masses and charges.

The ion drift-kinetic equation for the distribution function $f_a(\boldsymbol{X},t)$ for ion species a (with mass m_a and charge Z_a) is given by the following expression

* Corresponding author. Tel.: +1 609 851 7438; fax: + 1 505 665 7150.
E-mail address: rkolesni@pppl.gov (R.A. Kolesnikov).

0021-9991/$ - see front matter © 2010 Elsevier Inc. All rights reserved.
doi:10.1016/j.jcp.2010.04.018

$$\frac{D}{Dt}f_a \equiv \left(\frac{\partial}{\partial t} + \dot{\boldsymbol{X}} \cdot \frac{\partial}{\partial \boldsymbol{X}}\right) f_a = \sum_b C_{ab}[f_a, f_b]. \tag{1}$$

On the right hand side is the collision operator which includes self-collisions of ion species a as well as cross-collisions between various species. The guiding center coordinates $\boldsymbol{X} = (\boldsymbol{x}, \rho_\parallel, \mu)$ evolve according to the Lagrangian equations

$$\frac{d}{dt}\left(\frac{\partial}{\partial \dot{\boldsymbol{X}}} L_a\right) - \frac{\partial}{\partial \boldsymbol{X}} L_a = 0. \tag{2}$$

Here $\boldsymbol{x} = (r, \theta, \zeta)$ and r, θ and ζ are radial, poloidal and toroidal spatial coordinates correspondingly. The Lagrangian is given by $L_a = Z_a e \boldsymbol{p} \cdot \dot{\boldsymbol{x}} - H_a$. Here $\boldsymbol{p} = (p_r, p_\theta, p_\zeta)$ is canonical angular momentum and the Hamiltonian is

$$H_a = \frac{Z_a^2 e^2}{2m_a}\rho_\parallel^2 B^2 + \mu B + Z_a \Phi, \tag{3}$$

where magnetic moment $\mu = m_a v_\perp^2 / 2B$ ($\dot{\mu} = 0$ due to conservation of the adiabatic moment) and parallel gyroradius $\rho_\parallel = m_a v_\parallel / Z_a e\, B$ are expressed in terms of parallel and perpendicular velocities $v_\parallel$ and $v_\perp$. $\Phi(r)$ is the electric potential. The spacial part of $\dot{\boldsymbol{x}}$ may be rewritten in more conventional form as $\boldsymbol{v}_\parallel + \boldsymbol{v}_d$, where guiding center velocity $\boldsymbol{v}_d$ includes both the $-\nabla\Phi \times \boldsymbol{B}$ drift as well as gradient ∇B and curvature drifts in inhomogeneous magnetic field.

In δf algorithm [6–8], one solves the following equation for ion species a

$$\left(\frac{\partial}{\partial t} + \dot{\boldsymbol{X}} \cdot \frac{\partial}{\partial \boldsymbol{X}}\right) \delta f_a = -\dot{\boldsymbol{X}} \cdot \frac{\partial}{\partial \boldsymbol{X}} F_{0a} + \sum_b \left(C_{ab}[\delta f_a, F_{0b}] + C_{ab}[F_{0a}, \delta f_b]\right), \tag{4}$$

which is obtained directly from Eq. (1) by substituting $f_s = F_{0s} + \delta f_s$ and linearising the collision operator. F_{0s} is a time-independent shifted Maxwellian distribution function which satisfies

$$C_{ab}[F_{0a}, F_{0b}] = 0 \tag{5}$$

for any a and b.

The local shifted Maxwellian background distribution function is expressed in the following form [9,6]

$$F_{0a} \equiv F_{0a}(n_a, T, U_\parallel) = n_a \left(\frac{m_a}{2\pi T}\right)^{3/2} \exp\left[-\frac{m_a}{T}\left((v_\parallel - U_\parallel)^2/2 + \mu B\right)\right]. \tag{6}$$

Here $n_a(r) \equiv \langle n_a(r,\theta)\rangle$, $T(r)$ and $\omega_t(r) = [B/I(r)]U_\parallel(r,\theta)$ are experimentally given profiles for the ion density, temperature and toroidal angular frequency. These quantities together with $\Phi(t = 0)$ serve as initial conditions for our simulation. $I(r) = RB_\zeta$, where R is the major radius, B_ζ and B_θ are the toroidal and poloidal components of the magnetic field $\boldsymbol{B}$.

To satisfy the constraint Eq. (5) on background Maxwellian distribution functions, we must have the same ion temperature $T(r)$ and parallel flow $U_\parallel(r)$ profiles in the distribution functions (6) for all species. Experimentally observed temperatures $T_s(r)$ and toroidal angular frequencies $\omega_{ts}(r)$ might be different for different species s; this difference is captured by initial $\delta f_s(t = 0)$ in the following form

$$\delta f_s(t = 0) = F_{0s}(n_s, T_s, U_{\parallel s}) - F_{0s}(n_s, T, U_\parallel). \tag{7}$$

Our δf algorithm with linearized collision operator requires that $\delta f_s / F_{0s} \ll 1$. While temperature and parallel velocity profiles may be substantially different between different species, especially between ions and electrons, recent drift-kinetic simulations of realistic axisymmetric toroidal fusion devices show that this condition is well satisfied in deuterium plasmas in presence of carbon impurity [10,11].

Self-consistent ambipolar potential $\Phi(r)$ in general geometry is included via the equation [4]

$$\left(\langle|\nabla r|^2\rangle + 4\pi c^2 \sum_b n_b m_b \left\langle \frac{|\nabla r|^2}{B^2}\right\rangle\right) \frac{\partial^2 \Phi}{\partial t \partial r} = 4\pi \sum_b Z_b e \Gamma_b, \tag{8}$$

which is obtained from Ampere's equation. Angular brackets denote a flux surface average. The second term on the left hand side is the classical polarization current summed over species. The term on the right hand side is the radial current of ion guiding centers

$$\sum_b Z_b e \Gamma_s \equiv \sum_b Z_b e \left\langle \int d^3 v (\boldsymbol{v}_d \cdot \nabla r) \delta f_b \right\rangle. \tag{9}$$

In our algorithm we use the two-weight approach [5]. The first weight w is attached to each marker as a measure of the deviation of f_s from the fixed background F_{0s}. The need for the second weight p is motivated by the fact that in neoclassical simulations marker distribution function might also significantly deviate from the background F_{0s}. Defining the marker distribution function for species s in the extended phase space

$$g_s(\boldsymbol{X}, w, p, t) \sim \sum_i \delta(\boldsymbol{X} - \boldsymbol{X}_{si}(t))\delta(w - w_{si}(t))\delta(p - p_{si}(t)), \tag{10}$$

its kinetic equation may be written as follows

$$\frac{Dg_s}{Dt}+\frac{\partial}{\partial p}\left(\frac{dp}{dt}g_s\right)+\frac{\partial}{\partial w}\left(\frac{dw}{dt}g_s\right)=\sum_b C_{ab}[g_s,F_{0b}]. \tag{11}$$

The Eq. (4) for the evolution of δf_s as well as trivial equation for the background distribution function

$$\frac{DF_{0s}}{Dt}=0 \tag{12}$$

are reproduced when the following definitions for the marker particle weights w and p are adopted

$$\int dwwdpg_s=\delta f_s, \tag{13}$$

$$\int dwdp(1-p)g_s=F_{0s} \tag{14}$$

together with the following equations of motion for the two marker weights

$$\frac{dw}{dt}=\frac{1-p}{F_{0s}}\left(-\frac{DF_{0s}}{Dt}+\sum_b C_{sb}[F_{0s},\delta f_b]\right)-\eta(w-\bar{w}_s), \tag{15}$$

$$\frac{dp}{dt}=\frac{1-p}{F_{0s}}\left(-\frac{DF_{0s}}{Dt}\right)-\eta(p-\bar{p}_s). \tag{16}$$

Here η is the damping rate [12], which provides a continuous relaxation of w and p toward toward their locally average values $\bar{w}_s$ and $\bar{p}_s$. This procedure is introduced to reduce particle noise due to marker weight spreading without affecting physics results. Equations for δf_s and F_{0s} are not affected by these additional terms, which may be illustrated by substituting Eqs. (15) and (16) into Eq. (11) and taking moments Eqs. (13) and (14).

2. Unlike-particle collision operator

On the right hand side of Eq. (4), the linearised unlike-particle collision operator for species a colliding with species b can be rewritten as follows

$$C_{ab}[\delta f_a,F_{0b}]+C_{ab}[F_{0a},\delta f_b]\equiv C_{ab}^{TP}(\delta f_a)+C_{ab}^{FP}(\delta f_b). \tag{17}$$

The first term on the right hand side is the test-particle operator

$$C_{ab}^{TP}(\delta f_a)=\frac{\partial}{\partial \boldsymbol{v}}\cdot(\boldsymbol{v}F\delta f_a)+\frac{\partial^2}{\partial \boldsymbol{v}\partial \boldsymbol{v}}:\left(G\boldsymbol{I}+H\frac{\boldsymbol{vv}}{v^2}\right)\delta f_a \tag{18}$$

to describe the drag and diffusion part of the collisions. The coefficients

$$F=-v_{ab}\frac{v^3}{n_b}\frac{\partial}{\partial \boldsymbol{v}}H_b(\boldsymbol{v}), \tag{19}$$

$$G=v_{ab}\frac{v^2}{2n_b}\frac{\partial}{\partial v}G_b(\boldsymbol{v}), \tag{20}$$

$$H=v_{ab}\frac{v^3}{2n_b}\left(\frac{\partial^2}{\partial v^2}-\frac{1}{v}\frac{\partial}{\partial v}\right)G_b(\boldsymbol{v}) \tag{21}$$

are expressed in terms Rosenbluth's potentials

$$G_b(\boldsymbol{v})=\int d^3v'F_{0b}(v')|\boldsymbol{v}-\boldsymbol{v}'|, \tag{22}$$

$$H_b(\boldsymbol{v})=\left(1+\frac{m_a}{m_b}\right)\int d^3v'\frac{F_{0b}(v')}{|\boldsymbol{v}-\boldsymbol{v}'|}. \tag{23}$$

The collision frequency is defined by $v_{ab}=4\pi Z_a^2Z_b^2\Lambda_{ab}n_b/m_a^2v_a^3$. The standard Monte Carlo technique [13] is utilized in the drift-kinetic simulation to implement this operator.

The second term on the right hand side in Eq. (17) is the field-particle operator. This operator appears as a source term in Eq. (4), and not being sensitive to the details of δf_b, may be rewritten in the following form [15,14]

$$C_{ab0}^{FP}(\delta f_b)=\mathcal{R}_{ab}(v)v_\parallel\delta P_{ab}^0+\mathcal{Q}_{ab}(v)\delta E_{ab}^0 \tag{24}$$

Here, δP_{ab}^0 and δE_{ab}^0 are momentum and energy lost by species b test-particles as a result of collisions with species a field-particles

$$\delta P^0_{ab} = -\int d^3v m_b v_\parallel C^{TP}_{ba}(\delta f_b), \tag{25}$$

$$\delta E^0_{ab} = -\int d^3v (m_b v^2/2) C^{TP}_{ba}(\delta f_b). \tag{26}$$

Since test-particle collision operator conserves particle number, we remember that

$$\delta N^0_{ab} = -\int d^3v C^{TP}_{ba}(\delta f_b) = 0. \tag{27}$$

The functions $\mathcal{R}_{ab}$ and $\mathcal{Q}_{ab}$ are to be determined from the requirement that momentum and energy gained by species a field-particles must equal that lost by species b test particles

$$\int d^3v m_a v_\parallel C^{FP}_{ab}(\delta f_b) = \delta P^0_{ab}, \tag{28}$$

$$\int d^3v (m_a v^2/2) C^{FP}_{ab}(\delta f_b) = \delta E^0_{ab}. \tag{29}$$

With appropriate choices of multiplying factors, the functions $\mathcal{R}_{ab}$ and $\mathcal{Q}_{ab}$ may be found as follows:

$$\mathcal{R}_{ab}(v) v_\parallel = \frac{C^{TP}_{ab}(m_a v_\parallel F_{0a})}{\int d^3v' m_a v'_\parallel C^{TP}_{ab}\left(m_a v'_\parallel F_{0a}\right)}, \tag{30}$$

$$\mathcal{Q}_{ab}(v) = \frac{C^{TP}_{ab}\left(m_a v^2 F_{0a}\right)}{\int d^3v' (m_a v'^2/2) C^{TP}_{ab}(m_a v'^2 F_{0a})}. \tag{31}$$

The resulting operator Eq. (24) now satisfies conservation properties Eqs. (28) and (29). This can be verified by remembering that the test-particle operator preserves parity in $v'_\parallel$. Specifically, $C^{TP}_{ab}(m_a v'_\parallel F_{0a})$ is odd in $v'_\parallel$, and $C^{TP}_{ab}(m_a v'^2 F_{0a})$ is even in $v'_\parallel$.

Since we use Maxwellian background distribution functions, these expressions may be simplified by analytically computing the Rosenbluth potentials [13]:

$$\mathcal{R}_{ab}(v) = \frac{3\sqrt{\pi}}{4 n_a T}(1 + m_b/m_a)^{3/2} y_b^{-3/2} \phi(y_b), \tag{32}$$

$$\mathcal{Q}_{ab}(v) = \frac{\sqrt{\pi}}{2 n_a T}(1 + m_b/m_a)^{3/2} y_b^{-1/2} (m_a/m_b - d/dy_b)\phi(y_b), \tag{33}$$

where $\phi(y) = 2/\sqrt{\pi}\int_0^y e^t \sqrt{t}\, dt$ and

$$y_b = v^2/v_b^2 = m_b v^2/(2T). \tag{34}$$

As was illustrated by Sugama et al. [16], the test-particle C^{TP}_{ab} and field-particle C^{FP}_{ab0} operators defined by Eq. (24) and (24) satisfy the adjointness relations

$$\int d^3v \frac{\delta f_a}{F_{0a}} C^{TP}_{ab}(\delta g_a) = \int d^3v \frac{\delta g_a}{F_{0a}} C^{TP}_{ab}(\delta g_a), \tag{35}$$

$$\frac{T_a}{T_b}\int d^3v \frac{\delta f_a}{F_{0a}} C^{FP}_{ab0}(\delta f_b) = \int d^3v \frac{\delta f_b}{F_{0b}} C^{FP}_{ba0}(\delta f_a), \tag{36}$$

as well as Boltzmann's H-theorem

$$\frac{T_a}{T_b}\int d^3v \frac{\delta f_a}{F_{0a}}\left[C^{TP}_{ab}(\delta f_a) + C^{FP}_{ab}(\delta f_b)\right] + \int d^3v \frac{\delta f_b}{F_{0b}}\left[C^{TP}_{ba}(\delta f_b) + C^{FP}_{ba}(\delta f_a)\right] \leqslant 0, \tag{37}$$

which states the asymptotic relaxation of the distribution function to the local Maxwellian equilibrium state.

In Eq. (37), the left hand side vanishes when δf_s perturbations in the following form

$$\delta f_s = F_{0s}\left[\frac{\delta n_s}{n_s} + \frac{m_s}{T_s}\delta U_\parallel v_\parallel + \frac{\delta T_s}{T_s}\left(\frac{m_a v^2}{2T_a} - \frac{3}{2}\right)\right] \tag{38}$$

satisfy the correct null space of the linearized operator

$$C^{TP}_{ab}(\delta f_a) + C^{FP}_{ab}(\delta f_b) = 0. \tag{39}$$

Implementation of C^{FP}_{ab0} according to (24) within δf algorithm Eqs. (15) and (16) leads to unsatisfactory particle number conservation properties. This is due to the fact that, although test-particle operator conserves number according to Eq. (27), the field-particle operator Eq. (24) affects particle number moment $\int d^3v \delta f$ by altering δf according to Eq. (4). To obtain improved field-particle operator, one can use the procedure developed by Wang et al. [5] for iterative calculation of the field-particle conserving part in the following form

$$C^{FP}_{ab}(\delta f_b) = \sum_{n=0}^{N-1} C^{FP}_{abn}(\delta f_b) \tag{40}$$
$$C^{FP}_{abn}(\delta f_b) = \mathcal{H}_{ab}(v)\delta N^n_{ab} + \mathcal{R}_{ab}(v)v_{\|}\delta P^n_{ab} + \mathcal{Q}_{ab}(v)\delta E^n_{ab}.$$

An additional function $\mathcal{H}_{ab}$ is to be determined.

Operator (40) is implemented as a sequence of N iterations to enforce the appropriate conservation constraints. Specifically, the first $n = 0$ iteration enforces momentum and energy conservation according to Eqs. (28) and (29). Since simulation uses a finite number of markers, the consequent iterations are necessary to further improve momentum and energy (together with number) conservation properties according to

$$\delta N^n_{ab} = \int d^3v C^{FP}_{abn-1}(\delta f_b), \tag{41}$$
$$\delta P^n_{ab} = \int d^3v m_b v_{\|} C^{FP}_{abn-1}(\delta f_b), \tag{42}$$
$$\delta E^n_{ab} = \int d^3v (m_b v^2/2) C^{FP}_{abn-1}(\delta f_b). \tag{43}$$

Analogously to $\mathcal{R}_{ab}$ and $\mathcal{Q}_{ab}$ functions, the $\mathcal{H}_{ab}$ function is chosen to be

$$\mathcal{H}_{ab}(v) = 1 - \mathcal{Q}_{ab}(v), \tag{44}$$

so that the resulting operator Eq. (40) satisfies conservation properties Eqs. (41)–(43) as well as adjointness relation Eq. (36) and H-theorem Eq. (37). Self-adjointness and H-theorem in presence of contribution in Eq. (40) due to an additional $\mathcal{H}_{ab}(v)$ term can be demonstrated by remembering that the first ($n = 0$) iteration enforces conservation of number and energy leading to

$$\delta N^1_{ab} \int d^3v \frac{\delta f_a}{F_{0a}} \mathcal{H}_{ab}(v) = 0 \tag{45}$$

during the second ($n = 1$) iteration.

In Fig. 1, we show the time evolution of the radial electric field $E_r = -\partial\Phi/\partial r$ (at $r/a = 0.45$) as it approaches the steady state. The simulation was performed for deuterium-carbon two-species plasma in toroidal axisymmetric geometry with large-aspect ratio (major over minor radius, $R/a = 10$) and circular magnetic surfaces. The equilibrium magnetic field and major radius are $B = 3T$ and $R = 5$ m. The time is normalized to deuterium-deuterium collision frequency ν_{DD}. The ratios of thermal banana orbit width over typical density $n(r)$ and temperature $T(r)$ scale lengths are $\Delta_b/L_n \sim 0.25$ and $\Delta_b/L_T \sim 0.08$, respectively.

In this simulation, due to axisymmetric geometry, the unlike-particle collisions drive intrinsically ambipolar particle fluxes, and thus do not produce any radial current. Due to small electron/ion mass ratio, the electron radial currents are much smaller than the ion currents, and thus the electron contribution to ambipolar E_r dynamics is neglected. This would not be true in non-axisymmetric geometry, such as in a stelarator, where particle fluxes driven by unlike-particle collisions are not intrinsically ambipolar.

In Fig. 2, the evolution of $Z_s\Gamma_s$ from Eq. (9) is illustrated for both deuterium and carbon $s = D,C$. We verified that the ambipolar radial electric field reaches steady state when the total radial guiding center particle current (the right hand side of (8)) vanishes

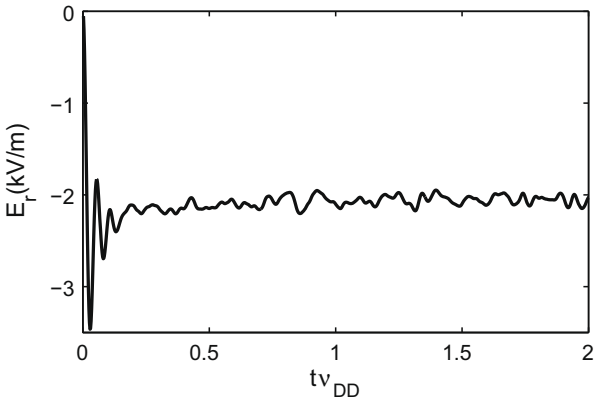

Fig. 1. Time dependence of the radial electric field.

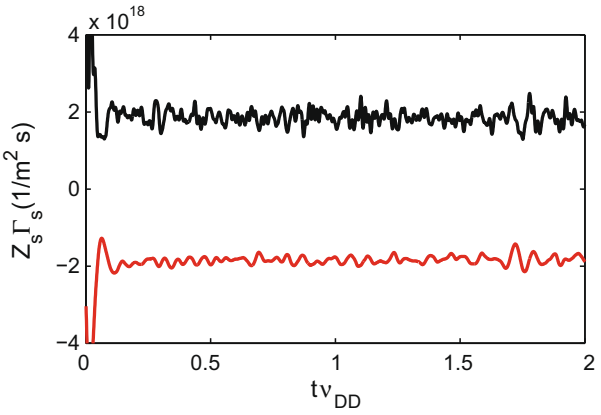

Fig. 2. Time dependence of $Z_s\Gamma_s$ for deuterium (black) and carbon (red). (For interpretation of the references to colour in this figure legend, the reader is referred to the web version of this article.)

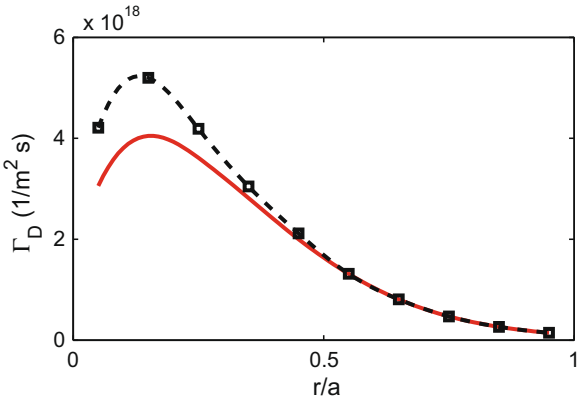

Fig. 3. Radial dependence of deuterium flux Γ_D versus normalized minor radius r/a.

$$\sum_s Z_s e \Gamma_s = 0, \tag{46}$$

while individual particle fluxes Γ_s stay finite.

In Fig. 3, the black dashed curve shows the steady state deuterium particle flux Γ_D versus normalized minor radius r/a. The red curve is the neoclassical estimate for the deuterium flux from Ref. [2]. The the black and the red curves are close to each other, except near the magnetic axis, where the discrepancy is due to the finite ion orbit size non-local effects [6,10,11].

3. Conservation properties

Fig. 4 shows the residual errors in number and energy. The blue and the red crosses (for deuterium and carbon) show the errors due to application of $C^{FP}_{ab0}(\delta f_b)$ operator Eq. (24), which enforces conservation of only momentum and energy. The resulting error in particle number is not satisfactory, which is the reason $C^{FP}_{ab}(\delta f_b)$ operator (40) needs to be used instead. Application of the complete operator (40) leads to improved residual error in particle number, which is comparable to residual errors in momentum and energy (squares in Fig. 4). Three-time ($N = 3$) recursive operations of C^{FP}_{ab} were used for this figure. Note that the deuterium component has slightly higher residual errors in all quantities compared to the carbon component due to higher thermal velocity.

While there is significant improvement in momentum and energy conservation when C^{FP}_{ab} is implemented, the residual errors will depend on the number of markers used in the simulation. It is difficult to have sufficient number of markers, especially for non-axisymmetric systems, for the error to converge. To resolve this problem, we follow the procedure developed by Satake [17] rewriting the field-particle operator in the following form

$$C^{FP}_{ab}(\delta f_b) = \mathcal{H}_{ab}(v)\delta N + \mathcal{R}_{ab}(v)v_\parallel \delta P + \mathcal{Q}_{ab}(v)\delta E. \tag{47}$$

Instead of using theoretical values for the functions δN, δP and δE, we find them from solving the following equation

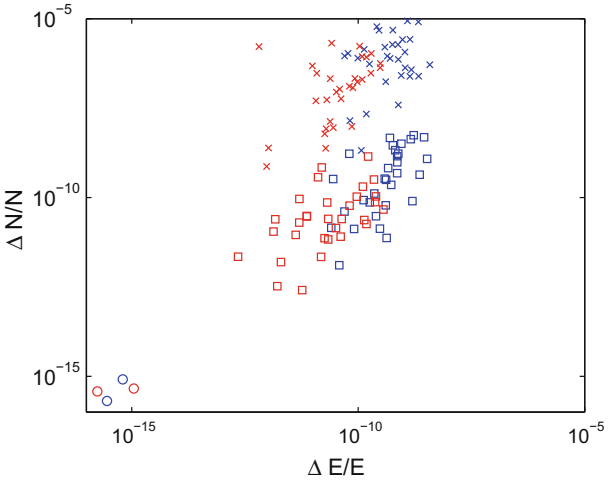

Fig. 4. Residual errors in energy and number for a set of sample simulation markers. The blue and the red markers are for deuterium and carbon, respectively. (For interpretation of the references to colour in this figure legend, the reader is referred to the web version of this article.)

$$m_a \int d^3v \begin{pmatrix} 1 \\ v_\parallel \\ v^2/2 \end{pmatrix} C_{ab}^{FP}(\delta f_b) = \begin{pmatrix} \delta N_{ab}^0 \\ \delta P_{ab}^0 \\ \delta E_{ab}^0 \end{pmatrix}, \tag{48}$$

which is a statement of conservation of number, momentum and energy Eqs. (27)–(29). For the simulation with a finite numer of markers, Eq. (48) may be rewritten as follows

$$\sum_{k=1}^{K}(1-p_k)\begin{pmatrix} \mathcal{H}_{ab} & \mathcal{R}_{ab}v_\parallel & \mathcal{Q}_{ab} \\ \mathcal{H}_{ab}v_\parallel & \mathcal{R}_{ab}v_\parallel^2 & \mathcal{Q}_{ab}v_\parallel \\ \mathcal{H}_{ab}v^2 & \mathcal{R}_{ab}v^2 v_\parallel & \mathcal{Q}_{ab}v^2 \end{pmatrix}_k \times \begin{pmatrix} \delta N \\ \delta P \\ \delta E \end{pmatrix} = -\begin{pmatrix} 0 \\ \delta P_{ab}^0/m_a \\ 2\delta E_{ab}^0/m_a \end{pmatrix}. \tag{49}$$

The Eq. (49) is designed to precisely enforce conservation of number, momentum and energy locally in configuration space. k is the parameter to sum over the total number of markers K in a cell of a spatial grid. In this procedure, this spatial grid must be chosen to be fine enough to resolve the profiles of equilibrium magnetic field and radial electric field. Using this approach, the error is at the rounding-error level (circles in Fig. 4) for both deuterium and carbon, independent of the number of markers in the simulation.

4. Thermal equilibration

In this section, we conduct a test of our unlike species collision operator by simulating thermal equilibration process in deuterium-carbon plasma. If deuterium and carbon both initially have Maxwellian distributions, but with different temperatures T_{D0} and T_{C0}, the equilibration process for carbon will be described by the following equation

$$\frac{dT_C}{dt} = -\bar{\nu}_\epsilon^{CD}(T_D - T_C), \tag{50}$$

with the total energy being preserved according to

$$n_C T_C + n_D T_D = n_C T_{C0} + n_D T_{D0}. \tag{51}$$

The relaxation frequency is given by

$$\bar{\nu}_\epsilon^{CD} = \frac{2}{3}\sqrt{\frac{2}{\pi}}\frac{m_C}{m_D}\left(\frac{T_C}{T_{C0}} + \frac{m_C}{m_D}\frac{T_D}{T_{C0}}\right)^{-3/2} \nu_{CD} \tag{52}$$

and $\nu_{ab} = 4\pi Z_a^2 Z_b^2 \Lambda_{ab} n_b / m_a^2 v_a^3$.

Figs. 5 and 6 show the time dependences of T_C/T_{C0} and $(T_C - T_D)/(T_{C0} - T_{D0})$ as the difference between deuterium and carbon temperatures vanished as a result of thermal relaxation brought by the collision operator. We use 10000 markers for both deuterium and carbon with $T_{C0}/T_{D0} = 0.5$ and $n_C/n_D = 0.85$, and simulation result agrees very well with the theory (50).

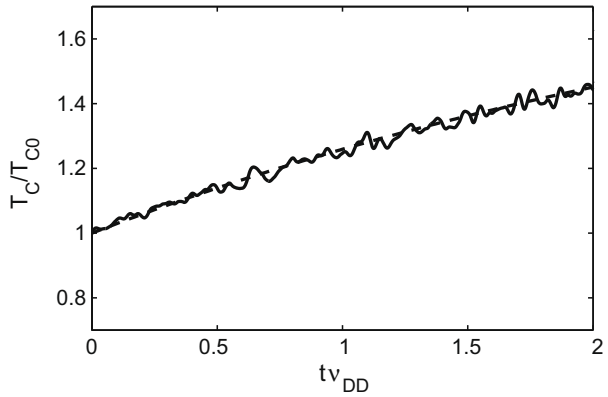

Fig. 5. Time dependence of normalized carbon temperature as the thermal equilibration occurs between carbon and deuterium. The solid curve is from simulation, the dashed curve is analytical prediction.

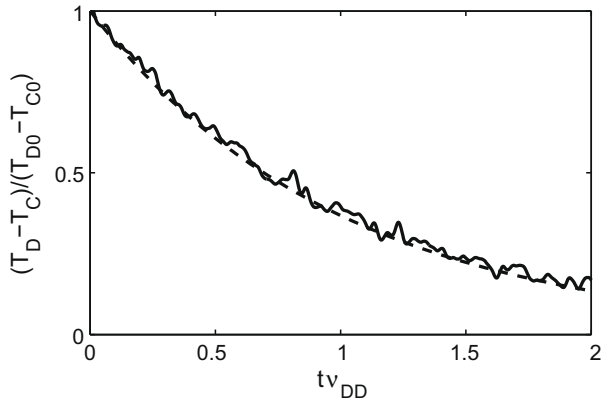

Fig. 6. Time dependence of $(T_C - T_D)/(T_{C0} - T_{D0})$. The solid curve is from simulation, the dashed curve is analytical prediction.

5. Conclusions

We developed a new unlike-particle collision operator for δf gyrokinetic particle simulation. This operator is necessary for self-consistent study of finite ion orbit effects in presence of impurities on neoclassical transport in toroidal plasmas. We described an algorithm for simulation of unlike-particle collisions in gyrokinetic framework. This includes test-particle and conserving field-particle parts. The field-particle operator is designed to enforce conservation of number, momentum and energy. It was shown that the new operator correctly simulates the thermal equilibration of different plasma components. It was verified that the ambipolar radial electric field reaches steady state when the total radial guiding center particle current vanishes.

Acknowledgment

This work was supported by U.S. DOE Contract No. DE-AC02-09CH11466.

References

[1] F.L. Hinton, R.D. Hazeltine, Rev. Mod. Phys. 48 (1976) 239.
[2] S.P. Hirshman, D.J. Sigmar, Nucl. Fusion 21 (1981) 1079.
[3] P. Helander, D.J. Sigmar, Collisional Transport in Magnetized Plasmas, Cambridge University Press, Cambridge, 2002 (Chapter 12).
[4] W.X. Wang, F.L. Hinton, K. Wang, Phys. Rev. Lett. 87 (2001) 055002.
[5] W.X. Wang, N. Nikajima, M. Okamoto, S. Murakami, Plasma. Phys. Control. Fusion 41 (1999) 1091.
[6] W.X. Wang, G. Rewoldt, W.M. Tang, et al, Phys. Plasmas 13 (2006) 082501.
[7] S.E. Parker, W.W. Lee, Phys. Fluids B 5 (1993) 77.
[8] W.W. Lee, Phys. Fluids 26 (1983) 556.
[9] F.L. Hinton, S.K. Wong, Phys. Fluids 28 (1985) 3082.
[10] R.A. Kolesnikov, W.X. Wang, F.L. Hinton, G. Rewoldt, W.M. Tang, PPCF 52 (2010) 042002.
[11] R.A. Kolesnikov, W.X. Wang, F.L. Hinton, G. Rewoldt, W.M. Tang, Phys. Plasmas 17 (2010) 022506.

[12] S. Brunner, E. Valeo, J.A. Krommes, Phys. Plasmas 6 (1999) 4504.
[13] X.Q. Xu, M.N. Rosenbluth, Phys. Fluids B 3 (1991) 627.
[14] Z. Lin, M.W. Tang, W.W. Lee, Phys. Plasmas 2 (1995) 2975.
[15] A.M. Dimits, B.I. Cohen, Phys. Rev. E 49 (1994) 709.
[16] H. Sugama, T.-H. Watanabe, M. Nunami, Phys. Plasmas 16 (2009) 112503.
[17] S. Satake, R. Kanno, H. Sugama, Plasma Fusion Res. 3 (2008) S1062.